Environmental Research 285 (2025) 122481

Contents lists available at ScienceDirect

Environmental Research

journal homepage: www.elsevier.com/locate/envres

# UV–activated peroxymonosulfate assisted heterotrophic ammonium assimilation for high–salinity leachate treatment: Mechanism and performance evaluation

Chuanfu Zhao [a,b], Wenhao Zhang [a,b], Jianhua Lei [a,b], Fei Han [a,b], Mengru Zhang [a,b], Yiting Guo [a,b], Yuke Li [c], Weizhi Zhou [a,b,*]

[a] School of Civil Engineering, Shandong University, Jinan, Shandong, PR China
[b] Laboratory of Water–sediment Regulation and Eco–decontamination, Jinan, Shandong, PR China
[c] Department of Water Management, Faculty of Civil Engineering and Geosciences, Delft University of Technology, Stevinweg 1, 2628 CN, Delft, the Netherlands

ARTICLE INFO

*Keywords:*
Heterotrophic ammonia assimilation
Advanced oxidation processes
Food waste leachate
Microbial network
Salinity

ABSTRACT

Food waste leachate is a high–strength wastewater characterized by refractory organics, high–salinity and elevated ammonium concentrations, posing challenges for effective treatment and nitrogen resource recovery. In this study, a novel strategy integrating UV/PMS advanced oxidation pretreatment with aerobic heterotrophic ammonium assimilation (HAA) was employed to enhance microbial nitrogen assimilation and carbon removal. Long–term monitoring revealed that the UV/PMS–HAA system achieved superior $NH_4^+$–N and COD removal efficiencies of 84.04 % and 90.74 % compared to the control. EPS analysis indicated higher protein content and tighter sludge structure, supporting improved microbial aggregation. Microbial diversity was significantly enhanced in the UV/PMS–HAA system, with enrichment of functional genera such as *Halomonas*, *Pseudomonas* and *Thauera*. Network and robustness analysis revealed intensified microbial cooperation and reduced disturbance sensitivity. Substantial upregulation of ammonium assimilation genes (*gdhA*, *glnA*, *gltB*), while nitrification–related genes (*amoA*, *hao*) were nearly absent, confirming a heterotrophic assimilation–dominated pathway. Enzyme activity analysis further supported this trend, with elevated *GS*, *GOGAT* activity and higher intracellular Glu, Gln, and TAA levels in the UV/PMS–HAA. UV/PMS pretreatment effectively reshaped microbial structure and function, promoting nitrogen recovery through assimilation rather than loss via nitrification, and provides a promising solution for treating complex nitrogen–rich wastewaters.

## 1. Introduction

The annual generation of food waste exceeds 60 million tons in large cities across China, yet the actual daily processing capacity does not exceed 14,000 tons, resulting in a processing efficiency of only 5.25 % (Lang et al., 2020). Large amounts of untreated food waste produce large amounts of leachate, which is harmful because of its high organic content, diverse chemical composition, high salinity, and possible contamination with heavy metals and pathogens (Zhang et al., 2025b). In recent years, various landfill leachate treatment technologies have been widely developed and applied. The pressure–driven membrane process can effectively throttle most contaminants, but the troublesome membrane contamination and high concentration of mother liquor reduce its cost performance (Garnier et al., 2023). Other physicochemical treatment methods (such as coagulation, adsorption, solidification) also only transfer pollutants from one phase to another (Zhang et al., 2021b). Most of the existing biodegradation processes are autotrophic nitrogen removal processes such as autotrophic nitrification and denitrification and anaerobic ammonia oxidation, which are inhibited by high organic concentration and high salinity (Li et al., 2018). Halophilic heterotrophic ammonia assimilation process (HAA) can effectively degrade leachate by converting carbon and nitrogen into nitrogen–containing organic matter at high salinity (Zhang et al., 2021a), but it needs pretreatment to improve biodegradability in the face of refractory organic wastewater (Zhao et al., 2023a). Lin et al. (2024) found assimilation phenomenon in the treatment of mature landfill leachate by HAA, but low carbon to nitrogen ratio leads to a large amount of nitrogen loss and retention of refractory organic matter.

* Corresponding author. School of Civil Engineering, Shandong University, Jinan, Shandong, PR China.
*E-mail address:* wzzhou@sdu.edu.cn (W. Zhou).

https://doi.org/10.1016/j.envres.2025.122481
Received 16 June 2025; Received in revised form 9 July 2025; Accepted 29 July 2025
Available online 5 August 2025

Lei et al. (2024) revealed that HAA process can realize the deep treatment of produced water containing sodium hexadecyl sulfonate and total petroleum hydrocarbons after pre–oxidation to break long carbon chains. The advanced integefficiencyd processes, such as the integration of AOP with biological processes, have achieved high processing efficiency and up to 32 % reduction in processing costs (Igwegbe et al., 2024), revealing the direction of future development.

Different types of high-salinity leachate wastewaters contain varying salt concentrations, and the microbial response to salinity is highly dependent on the specific salinity level. Saline wastewater is typically defined as having a salinity above 1 % (w/w), with an average concentration around 3 % (w/w) (Srivastava et al., 2021). Elevated salinity imposes high osmotic stress on ordinary freshwater microbial cells, leading to water efflux, cytoplasmic shrinkage, and in severe cases, cell dehydration and death, thereby impairing pollutant removal efficiency. Halotolerant heterotrophic ammonia assimilation microbes derived from marine sediments exhibited inhibited activity under no-salt conditions (<1 %), satisfactory performance under low and moderate salinity (1–7 %), and signs of stress when exposed to high-salinity conditions (>7 %) (Gao et al., 2023; Zhang et al., 2022; Zhao et al., 2024b). Microorganisms cope with high salinity primarily by accumulating compatible solutes (e.g., betaine, proline, and trehalose) and regulating the uptake of inorganic ions to maintain intracellular osmotic balance without disrupting cellular metabolism (Gunde-Cimerman et al., 2018). The excellent performance of halophilic HAA microorganisms lays the foundation for resistance to high salt shock and tolerance to residual free radical oxidation.

The advanced oxidation processes (AOP) can remove color and refractory organic matter, improved the biodegradability of leachate through effective free radicals (Masouleh et al., 2024). Peroxomonosulfate (PMS) is a kind of green oxidant with low price and good environmental durability, produced hydroxyl radical (•OH) and sulfate radical ($SO_4^{\bullet-}$) through energy input excitation and electron transfer, further treat refractory organic matter (Sun et al., 2024). Based on the summarized data in Table S1, various persulfate-based advanced oxidation processes exhibit differing efficiencies in treating landfill leachate, depending on operational conditions and wastewater characteristics. Biochar-mediated activation, while considered a more sustainable alternative, has been reported to release dissolved organic carbon during the process, which can scavenge reactive oxygen species and affect overall degradation efficiency (Yang et al., 2025). Transition metal-activated PMS exhibits ideal removal efficiency but often involves rate-limiting complexation and secondary metal pollution (Wang and Wang, 2018). Ultraviolet (UV)–based AOPs are considered a mature technology due to the ease of installation and operation of UV systems in current water and wastewater treatment plants (Gao et al., 2025). UV–activated PMS has the advantages of simple operation and no secondary pollution, which is different from thermal or metal cation activation methods (Cai et al., 2022). In the UV/PMS system, dissolved organic matter (DOM) degradation is mainly carried out by dealkylation, decarboxylation, hydrogenation and dearomatization, but high–salt ions such as high concentrations of Cl– weaken these reactions, and are replaced by chlorinated DOM through chlorine addition/substitution and other oxidation reactions (Zhao et al., 2025a), thus resulting in incomplete degradation of organic matter (Zhao et al., 2025b). Therefore, biodegradation as a further processing process of AOP is very necessary. The refractory organic matter is transformed from long chain to small molecule short chain organic matter, and retains nutrients for heterotrophic microorganisms to achieve integrated removal of carbon, nitrogen and phosphorus.

Herein, the advanced treatment and nutrient recovery of high–salt wastewater were realized by constructing the UV/PMS–HAA coupling system for the treatment of food waste leachate. The objective of this study was to (1) determine the optimal oxidant dose and UV activation time for COD degradation in leachate treated with UV/PMS; (2) systematically explore the effects of UV/PMS pretreatment settings on the removal of pollutants in the long–term operation of heterotrophic ammonia assimilation; (3) reveal the effects of pre–oxidation on microbial community interaction and aggregation.

## 2. Materials and methods

### 2.1. Batch tests

The food waste leachate used in this study was collected from a university canteen in Jinan. The concentration ranges of major pollutants in leachate were 3200–3800 mg/L COD, 130–160 mg/L $NH_4^+$–N, and 3–3.5 % salinity. The UV/PMS oxidation system consisted of a reactor equipped with a UV lamp (254 nm, 40 W). The reaction was carried out in a beaker with a working volume of 0.5 L, maintaining a working temperature of 25 °C. The initial pH of the leachate was adjusted to 7.0. Magnetic stirring was applied to ensure homogenous mixing. Different PMS concentrations (0, 0.2, 0.5, 1, 2, 3, and 4 mM), UV radiation intensities (20, 30, 40, 50, 60W) and radiation distances (5, 20, 50, 100, 300 cm) were tested to evaluate the oxidation efficiency. The control tests without UV and PMS were established to verify the contribution of physical adsorption. The masking tests were established to verify the oxidative contribution of free radicals by adding tert butyl alcohol (TBA) and ethanol (EtOH). Samples were collected at predetermined time intervals and filtered using 0.45 μm membranes for determination of COD, TN, $NH_4^+$–N, $NO_2^-$–N, and $NO_3^-$–N. In the batch optimization tests, the HAA process was conducted in a 0.5 L beaker with aeration (DO 5–8 mg/L) over 24 h using 5 g/L sludge from a stable pilot-scale reactor. The inoculated sludge was obtained from a stable HAA pilot scale bioreactor with a corresponding sludge concentration of 5 g/L. The biodegradability of the pre–oxidation effluent was judged by the final effect of the pre–oxidation coupled with biodegradation under different conditions. The degradation efficiency of organic pollutants was assessed by measuring COD removal. The nitrogen balance verification tests were performed to verify nitrogen assimilation in HAA processes with and without UV/PMS pretreatment. 30 mg/L allyl thiourea (ATU) was added to shield the potential effects of ammonia oxidation. Pollutant concentrations were monitored over time, and total nitrogen in biomass and supernatant was analyzed following Zhang et al. (2025a).

### 2.2. Coupled system construction of long-term operation

Following the UV/PMS pre–oxidation, the treated leachate was introduced into an HAA bioreactor. Two 1 L cylindrical sequential batch reactors (SBRs) were employed: one receiving UV/PMS–treated leachate (test group) and another receiving untreated leachate (control group). The optimum oxidant dose and activation time of UV/PMS in the long–term experiment was determined to be the best conditions for the batch experiment, while the food waste leachate content, the aeration conditions and sludge inoculation conditions of the HAA biodegradation reactor were the same as those of the batch experiment. The hydraulic retention time was maintained at 24 h.

### 2.3. Microbial community

Samples for microbial community analysis was collected from the bioreactors on days 0, 30, 60, and 90. Bacterial genomic DNA was extracted from the sludge samples using the PowerSoil DNA Separation Kit (MoBio Laboratories, Carlsbad, CA, USA). The bacterial 16S rRNA gene fragments were amplified using primer pairs 515F (GTGCCAGCMGCCGCGGTAA) and 806R (GGACTACHVGGGTWTCTAAT). The microbial sequencing results (raw data) are available in the National Center for Biotechnology Information (NCBI) database under the number PRJNA1257394. Bioinformatic–based microbial community analysis methods refer to the previous study (Zhao et al., 2024a), including microbial co–occurrence networks, ZIPI analysis, robustness

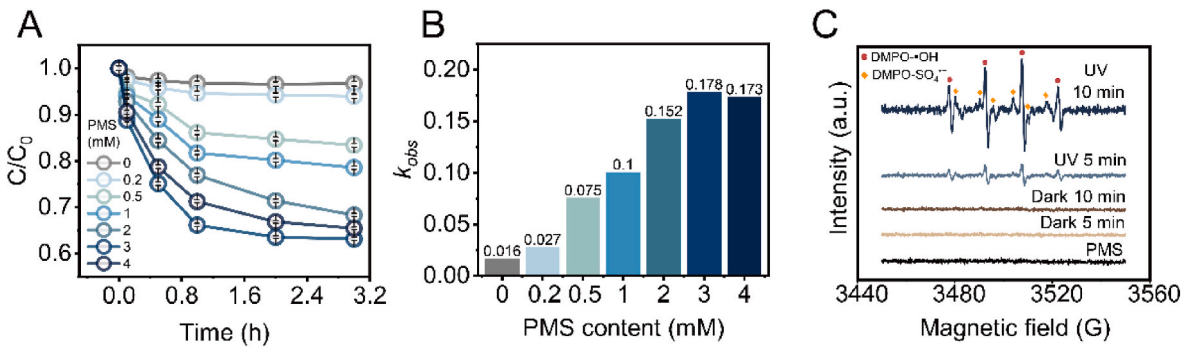


**Fig. 1.** (A) COD degradation performance in only UV/PMS system of different PMS dosage. (B) The $k_{obs}$ of only UV/PMS system in different PMS dosage. (C) EPR experiment to identify highly active radicals. Reaction conditions: $[PMS]_0 = 3$ mM.

analysis, habitat specialization, neutral community, null model calculations, niche breadth, similarity percentage (SIMPER), Procrustes analysis, mantel analysis, and partial least squares pathway modeling (PLS–PM).

### 2.4. Analytical methods

The concentrations of COD, TN, $NH_4^+$–N, $NO_2^-$–N, and $NO_3^-$–N were determined using standard methods. The radicals ($SO_4^{\bullet-}$ and •OH) were captured with DMPO in water and analyzed using electron paramagnetic resonance spectroscopy (EPR, Bruker EMXplus-A300, Germany). The extraction protocol and electrochemical characterization of

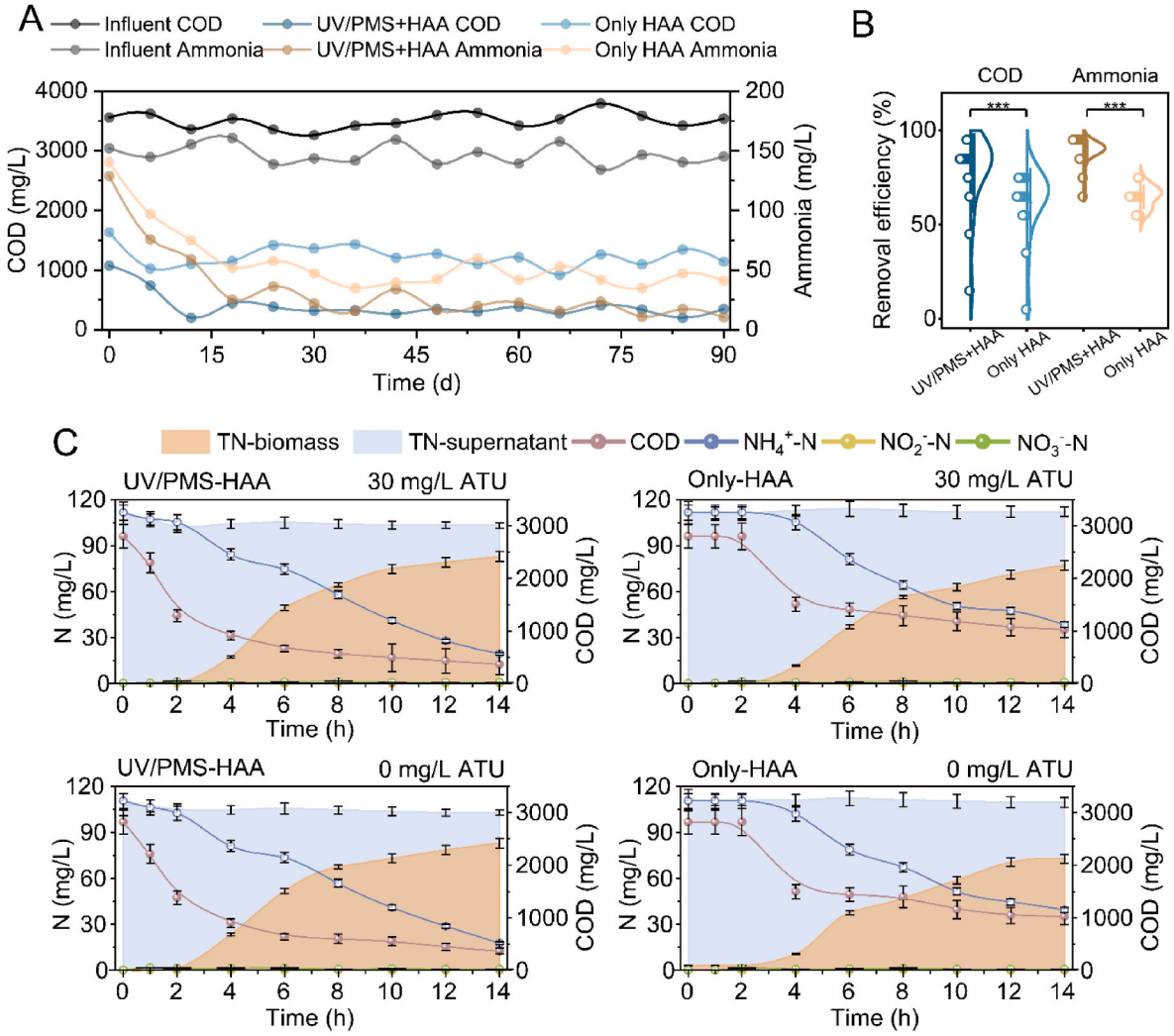


**Fig. 2.** Long-term performance of UV/PMS coupled HAA system and only HAA system under optimal PMS dosage and UV activation time: (A) pollutant concentration variation and (B) pollutant removal efficiency. (C) Batch tests on nitrogen balance of UV/PMS coupled HAA system and UV/PMS only system with 30 mg/L ATU addition and 0 mg/L ATU addition.

extracellular polymeric substances (EPS) with an electrochemical workstation (CHI760E, CH Instruments, China), including cyclic voltammetry (CV), linear sweep voltammetry (LSV), differential pulse voltammetry (DPV) and electrochemical impedance analysis (EIS), are shown in Text S1. Three–dimensional fluorescence spectrum (3D–EEM) analysis parameters refer to previous studies (Qin et al., 2025), and parallel factor analysis (PARAFAC) is used to further component analysis (Zhao et al., 2021). The concentrations of polysaccharides (PS) and proteins (PN) in the EPS were determined by the anthrone-sulfuric acid method and the modified Lowry method, respectively (Zhao et al., 2022). Functional groups and chemical bonds were analyzed through Fourier Transform Infrared Spectroscopy (FTIR) using the Thermofisher Nicolet iS 50 instruments, covering a range of 500–4000 $cm^{-1}$. The protein secondary structure was analyzed by the deconvolution fitting of the amide I region of FTIR using Peakfit software (Zhao et al., 2025b). Glutamate dehydrogenase (*GDH*), glutamine synthetase (*GS*), glutamine synthase (*GOGAT*), total amino acids (*TAA*), glutamine (*Gln*), and glutamate (*Glu*) in sludge were quantified using corresponding assay kits (Solarbio, Beijing, China).

## 3. Results and discussion

### 3.1. Optimization of oxidation conditions for UV/PMS Pre–Treatment

To determine the optimal oxidation conditions, batch tests were conducted to evaluate the influence of PMS concentration and reaction time on organic pollutant degradation. In Fig. 1A, the degradation efficiency increased significantly with PMS dosage, particularly from 0.2 to 3 mM, while a slight decrease was observed at 4 mM. The results were attributed to radical scavenging effects, where excessive PMS leaded to self–quenching reactions (Eqs. (1)–(3)), reducing the concentration of active radicals (Zhao et al., 2025b). Table S2 presents a comparison of the fitting performance of zero-order, first-order, and second-order kinetic models for UV/PMS degradation under different PMS dosages. The results indicated that the first-order model provided a more comprehensive representation of the degradation process, especially when the oxidative effect of PMS was pronounced. The reaction efficiency constant ($k_{obs}$) and coefficient of determination ($R^2$) derived from the first–order kinetic model (Fig. 1B and Fig. S1) further confirmed that 3 mM PMS achieved the highest degradation efficiency, indicating an optimal oxidant concentration. The COD removal efficiency increased significantly within the first 2 h, indicating that sufficient reactive species were generated to degrade complex organic matter into bioavailable intermediates. Extending the activation time beyond 2 h resulted in only marginal improvements, suggesting that excessive UV exposure may lead to radical scavenging or unnecessary energy consumption. Therefore, a 2-h UV activation period was determined to be the optimal balance between efficiency and energy input. Additionally, UV treatment efficiency improved with increasing intensity, but no significant differences were observed beyond 40 W (Fig. S2A). Therefore, 40 W was chosen as the optimal setting considering both performance and energy consumption. The variations in radiation distance (5–300 cm) showed minimal influence on removal efficiency (Fig. S2B).

Fig. 1C shows EPR spectra confirming the generation of hydroxyl radicals (•OH) and sulfate radicals ($SO_4^{\bullet-}$) during UV/PMS activation. No signals are observed in dark or PMS-only controls. The radical signal intensity increases with UV exposure time, confirming •OH and $SO_4^{\bullet-}$ as the dominant species in the UV/PMS system. In Fig. S2C and D, masking tests (adding EtOH and TBA) and control tests (excluding UV and PMS) proved that the degradation of COD was mainly attributed to • OH and $SO_4^{\bullet-}$, and excluded the physical adsorption of COD and $NH_4^+$–N by the UV/PMS system. Fig. S3 shows that PMS pre-oxidation enhanced COD removal by HAA. Moderate PMS (0.2–3.0 mM) improved biodegradability (70–80 % COD removal), while higher doses (3.0–4.0 mM) exceeded 80 % but further improvement was minimal. Excessive PMS may lead to partial mineralization or the formation of refractory byproducts, reducing biodegradability, or that residual PMS inhibited microbial activity (Yin et al., 2024). An optimal PMS concentration (3.0 mM) was identified, balancing oxidation efficiency and microbial activity.

$$HSO_5^- + hv \rightarrow SO_4^{\bullet-} + \cdot OH \quad (1)$$

$$SO_4^{\bullet-} + SO_4^{\bullet-} \rightarrow S_2O_8^{2-} \quad (2)$$

$$\cdot OH + \cdot OH \rightarrow H_2O_2 \quad (3)$$

### 3.2. Long–term performance of the UV/PMS–HAA system

Following the batch tests to determine optimal oxidation conditions (3 mM PMS and 2 h UV), a long–term continuous operation was conducted to evaluate the combined effect of UV/PMS pre–oxidation and HAA on pollutant removal. In Fig. 2A and B, COD removal in the UV/PMS–HAA system was significantly higher than in the Only HAA. Over the 90–day operation, UV/PMS–HAA achieved a stable COD removal efficiency of 90.74 %. In contrast, the Only HAA exhibited a lower COD removal efficiency of 67.50 %, resulting in a residual COD of approximately 1236.9 mg/L. UV/PMS oxidation alone did not completely mineralize organic pollutants but rather converted them into biodegradable intermediates, which required microbial assimilation for further degradation (Zhao et al., 2023a). The UV/PMS–HAA system achieved higher $NH_4^+$–N removal (84.04 %) than HAA alone (67.50 %), due to oxidative pretreatment enhancing carbon/nitrogen bioavailability. The masking tests and control test (Fig. S2) proved contribution of the main pollutant degradation by • OH and $SO_4^{\bullet-}$, and excluded the physical adsorption contribution of UV/PMS to the main pollutants. UV/PMS broke down complex organics in leachate into smaller compounds, promoting microbial assimilation via GS and GDH pathways and improving overall nitrogen removal (Babu Ponnusami et al., 2023; Yin et al., 2024).

In the absence of oxidative pre-treatment, the organic pollutants in leachate remained in more complex molecular forms, limiting microbial degradation. The pretreated wastewater contained more accessible nitrogen and carbon sources, allowing for a more efficient heterotrophic nitrogen assimilation process. The improved nitrogen removal in the UV/PMS–HAA system was attributed to the enhanced availability of biodegradable organic substrates, which promoted microbial nitrogen assimilation through the glutamine synthetase and glutamate dehydrogenase pathways (Qin et al., 2025). While UV/PMS effectively broke down complex macromolecular organics into smaller intermediates, the subsequent microbial process ensured their complete degradation and nitrogen incorporation, leading to more stable and efficient pollutant degradation compared to standalone UV/PMS treatment.

### 3.3. Nitrogen balance tests

To verify that ammonia removal in the UV/PMS–HAA system was primarily due to heterotrophic ammonia assimilation rather than nitrification, a nitrogen balance experiment was conducted using 30 mg/L ATU as a nitrification inhibitor. Fig. 2C presents the nitrogen transformation dynamics in both the UV/PMS–HAA system and the HAA–only system under conditions with and without ATU. In the UV/PMS–HAA system, $NH_4^+$–N removal was consistent regardless of ATU addition with over 80 % reduction observed within 12 h. Meanwhile, TN in the supernatant decreased progressively, while TN in biomass increased proportionally, indicating active microbial assimilation. The negligible accumulation of nitrite and nitrate further supported that nitrification was not the primary nitrogen removal pathway. The COD reduction trend was closely aligned with ammonia removal, reinforcing the coupling between organic carbon metabolism and nitrogen assimilation. In the HAA–only system (without UV/PMS pre–oxidation), $NH_4^+$–N removal was still primarily attributed to microbial assimilation

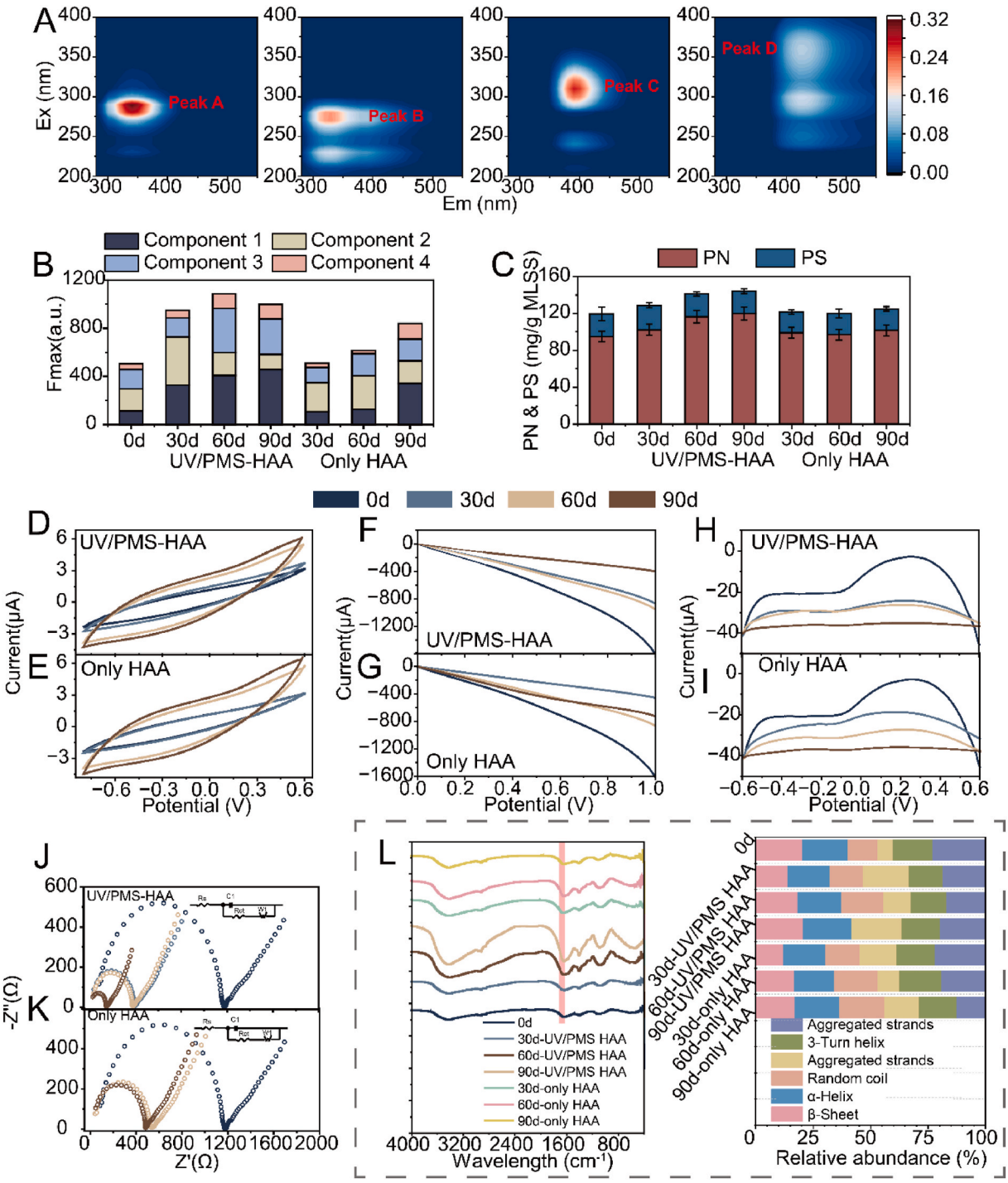


**Fig. 3.** Extracellular polymeric substances (EPS) based on EEM-PARAFAC: (A) Main fluorescence components and (B) Fmax proportion. (C) Polysaccharide and protein contents of EPS. Electrochemical analysis of EPS: (D–E) CV test, (F–G) LSV test, (H–I) DPV test, and (J–K) EIS test. (L) FTIR spectrograms and protein secondary structures of EPS.

rather than nitrification, as ATU addition had no inhibitory effect on ammonia removal. However, the ammonia removal efficiency was slightly lower compared to the UV/PMS–HAA system, likely due to the absence of UV/PMS pre–treatment. The relatively slower COD removal in this system suggested that the availability of biodegradable organic carbon was a limiting factor in microbial nitrogen assimilation.

### 3.4. Microbial extracellular polymeric substances

#### 3.4.1. EEM– PARAFAC

The PARAFAC–EEM analysis revealed distinct changes in EPS composition over time and components 1–4 was distinguished (Fig. 3A and B and Fig. S4). Correspondingly, the main fluorescence peak A (wavelength/emission wavelength, 280/350 nm), peak B (275/325 nm), peak C (300/400 nm) and peak D (350/425 nm) were identified as humic–like, aromatic proteins, fulvic acid–like proteins and tryptophan proteins, respectively (Zhao et al., 2025b). In the UV/PMS–HAA system,

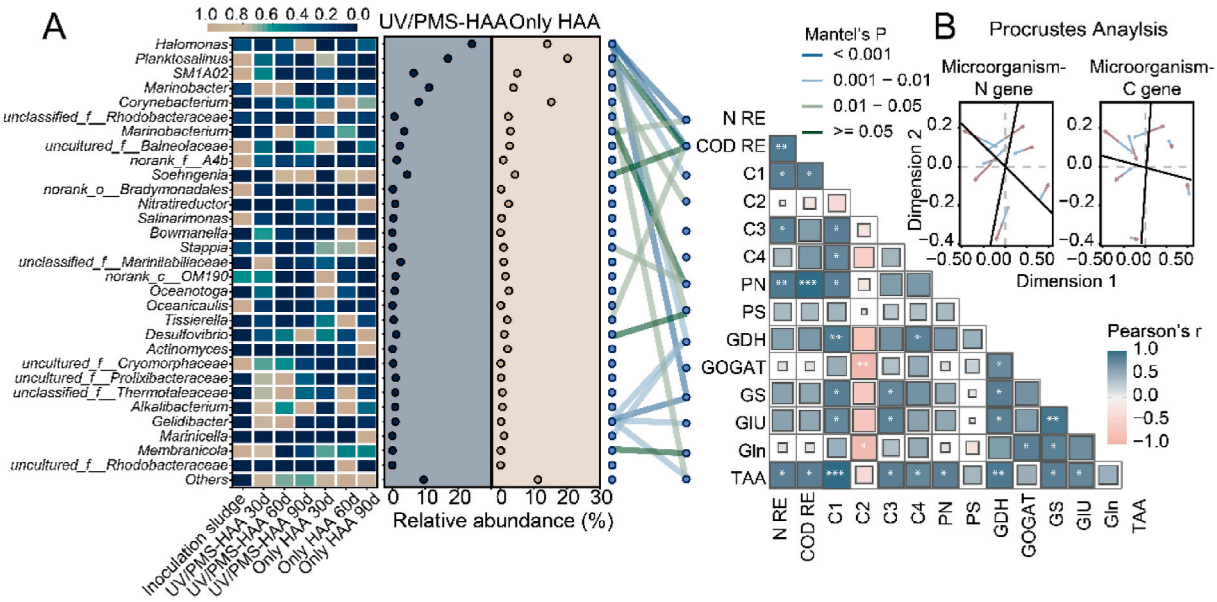


**Fig. 4.** (A) Correlation analysis of microbial communities and environmental factors: Relative abundance at genus level; Mental test analysis with operational conditions effects on the evolution of microbial community and functional genes & enzyme. (*p < 0.05; *p < 0.01, ***p < 0.001); (B) Pairwise correlation analyses based on the Bray-Curtis matrix for nitrogen, carbon, and microorganism using Procrustes analysis. The forward path coefficients are indicated by red arrows. These associations were determined through Mantel tests and visualized based on significance thresholds, with line colors denoting Mantel's P values (blue for <0.001, teal for 0.001–0.01, light green for 0.01–0.05, and dark green for ≥0.05). (For interpretation of the references to color in this figure legend, the reader is referred to the Web version of this article.)

humic–like substances (Component 1) increased significantly from 113.7 to 457.3 a.u., indicating enhanced organic matter transformation via radical–induced oxidation (Zhao et al., 2023a). Tryptophan–like proteins (Component 4), a marker of microbial activity, also rose from 46.5 to 120.6 a.u., suggesting stimulated microbial metabolism. In contrast, the only–HAA system showed smaller increases in Components 1 and 4, indicating limited EPS evolution. PMS pre–oxidation promoted EPS complexity and microbial response.

### 3.4.2. Component determination of EPS

In Fig. 3C, the variation of EPS, including PN and PS contents, was quantitatively analyzed to evaluate microbial response under different treatment conditions. In the UV/PMS–HAA system, PN concentration increased steadily from 94.8 ± 5.7 mg/g MLSS at day 0–119.8 ± 7.2 mg/g MLSS at day 90, representing a 26.4 % enhancement. This increase may be due to the generation of more readily biodegradable substrates by PMS oxidation, which stimulated microbial growth and EPS secretion. In contrast, the PS content remained relatively stable throughout the operation (24.6 ± 7.4 to 24.2 ± 2.4 mg/g MLSS). The protein components played a more dominant role in the structural and functional adaptation of EPS (Zhao et al., 2023b). In the only–HAA system, a less pronounced increase in PN was observed, reaching 101.5 ± 6.1 mg/g MLSS by day 90. Meanwhile, PS content fluctuated slightly within a narrow range (22.5–23.4 mg/g MLSS). UV/PMS pre–oxidation step promoted EPS protein secretion, contributing to improved system stability and pollutant removal efficiency.

### 3.4.3. Electrochemical characterization of EPS

Electrochemical analyses, including CV, LSV, DPV, and EIS, were conducted to assess the electrochemical characterization of EPS extracted from both systems (Fig. 3D–K). In the UV/PMS–HAA system, CV curves showed a progressive increase in current response from day 0 to day 90, indicating enhanced redox activity of EPS (Zhao et al., 2025a). This trend was further confirmed by LSV results, where a higher current output was observed at each time point compared to the only–HAA group. Similarly, the only–HAA system showed modest improvements in current generation, but the magnitude remained consistently lower, suggesting limited electroactive compound accumulation. DPV analysis revealed increased electrochemical activity of EPS over time, especially in the UV/PMS–HAA. A higher oxidative peak current at 90 days indicated enhanced electron transfer capacity, suggesting strong heterotrophic microbial oxidation and utilization of organic matter. In contrast, the Only HAA group showed a weaker response, suggesting less stimulation of redox–active EPS components. EIS analysis further supported these observations. The UV/PMS–HAA system showed a gradual decrease in charge transfer resistance ($R_{ct}$) over time, indicating improved electron mobility within the EPS matrix. In contrast, the only–HAA system exhibited relatively stable and higher $R_{ct}$ values. UV/PMS pretreatment facilitated the enrichment of carbon oxidation substrate in EPS, thereby enhancing electron transfer processes crucial for pollutant biodegradation and system performance.

### 3.4.4. Protein secondary structure base on FTIR of EPS

Fig. 3L illustrated the FTIR spectra of EPS samples in UV/PMS–HAA and Only HAAs, reflecting the presence and transformation of key functional groups of EPS during UV/PMS–HAA treatment. Characteristic amide I and amide II bands (around 1650 $cm^{-1}$ and 1540 $cm^{-1}$) were consistently detected associated with peptide bonds to reflect C=O stretching and N–H bending vibrations, confirming the abundance of protein–related structures. Additionally, broad O–H and N–H stretching bands in the 3200–3400 $cm^{-1}$ region, as well as C–O–C and C–O–H vibrations near 1000–1100 $cm^{-1}$, revealed the presence of polysaccharides. The changes in peak intensity and profile over time suggest that the composition and structure of EPS evolved during operation, driven by advanced oxidation residual stress and microbial adaptation, with proteins and polysaccharides jointly contributing to matrix functionality.

The amide I region (1600–1700 $cm^{-1}$) (Fig. S5) identified six secondary structures in EPS: β–sheet, α–helix, random coil, aggregated strands, 3–turn helix, and antiparallel β–sheet/aggregated strands. Initially, β–sheet (20.30 %) and antiparallel strands (22.95 %) dominated, indicating a stable, ordered EPS conformation. After 30 days of UV/PMS–HAA treatment, β–sheet content declined to 13.94 %, while random coil and aggregated strands increased, suggesting oxidative

stress disrupted protein folding. By day 60, β–sheet (18.22 %) and random coil (18.44 %) levels indicated partial recovery and microbial adaptation. At day 90, β–sheet (20.59 %) and α–helix (21.23 %) returned to or exceeded initial values, and random coil disappeared, reflecting restored protein integrity and stabilized EPS structure. UV/PMS oxidation enhanced the functional structure of EPS, reflecting microbial resilience and improved sludge stability under oxidative stress.

### 3.5. Microbial community succession

Microbial community analysis could provide insights into the functional stability, adaptability, and ecological mechanisms underpinning system performance. Alpha diversity index (Fig. S6) showed that the Chao1 and ACE values in the UV/PMS-HAA were significantly higher than those in the Only HAA, and Shannon and Simpson index within the UV/PMS-HAA increased, indicating increased microbial richness following PMS oxidation. The generation of diverse ecological niches under oxidative stress promoted the coexistence of multiple taxa with distinct functional traits. At phylum (Fig. S7), the inoculation sludge was dominated by Bacteroidota (47.8 %), followed by Proteobacteria (26.7 %) and Planctomycetota (17.8 %). Over time, UV/PMS–HAA treatment significantly enriched Proteobacteria, reaching 55.1 % at 90 days, while Bacteroidota declined sharply to 6.8 %. In contrast, the Only HAA group showed slower *Proteobacteria* enrichment (from 21.2 % to 45.0 %) and retained higher Actinobacteriota and Firmicutes abundances, suggesting a more fermentative and less oxidative microbial profile.

At genus level (Fig. 4A), the community in the inoculation stage was dominated by *Planktosalinus* (41.7 %), *Halomonas* (18.1 %), and *SM1A02* (15.9 %), which were typically associated with halophilic or moderately halotolerant traits. *Planktosalinus* was known for polysaccharide degradation under microaerophilic conditions (Qin et al., 2025), making it well–suited for initial organic matter breakdown in high–organic–strength leachate. However, under UV/PMS–HAA conditions, the relative abundance of *Planktosalinus* was drastically declined to only 1.3 % at day 90, suggesting that the oxidative stress induced by PMS–derived reactive oxygen species (ROS) limited its survivability and metabolic activity (Jiao et al., 2024). In contrast, *Halomonas* showed a different response under UV/PMS–HAA. Although its abundance decreased initially (9.9 % at 30 d), it became the dominant genus at 90 d (48.3 %). *Halomonas* were well–documented for their salt tolerance, metabolic versatility, and aerobic ammonia assimilation capacity (Zhao et al., 2025b). The enrichment of this genus likely reflected a competitive advantage under high–ROS and high–salinity conditions, supporting both COD removal and nitrogen transformation through robust oxidative metabolism (Zheng et al., 2025). *Marinobacter*, another halotolerant genus with hydrocarbon–degrading and denitrifying capabilities (Zhang et al., 2021b), was highly enriched during early UV/PMS–HAA operation (19.7 % at 30 d), though it declined sharply at day 90 (0.86 %). The initial proliferation of this genus suggested a role in early–stage oxidative degradation of organic compounds, particularly under the selective pressure of UV/PMS treatment, but its decrease at later stages indicates possible competitive exclusion by *Halomonas* or other redox–active genera better adapted to stabilized conditions. *Corynebacterium* was more abundant in the Only HAA group, peaking at 28.1 % at 60 d. While some *Corynebacterium* were facultatively anaerobic and capable of amino acid metabolism, their high abundance may reveal the accumulation of proteinaceous compounds in systems lacking pre–oxidation (Zhao et al., 2024a). The proliferation of *Soehngenia* and *Tissierella* in both groups (e.g., 9.2 % and 0.83 % at 90 d under UV/PMS–HAA) suggested a role for these fermenters in residual organic matter degradation (Khanthong et al., 2021). However, their abundance remained lower in the UV/PMS–HAA compared to the Only HAA group, which could be attributed to the oxidative pre–treatment inhibiting its niches. Interestingly, *Marinobacterium* displayed a transient dominance at 60 d under UV/PMS–HAA (12.6 %) before declining at 90 d. As a genus involved in hydrocarbon degradation and nitrogen cycling (Zhao et al., 2024b), its temporal dynamics may reflect ecological succession during biofilm maturation under oxidative stress.

LEfSe analysis (Fig. S8) revealed distinct microbial communities and functional specialization between UV/PMS–HAA and Only HAAs. *Halomonas*, *Marinobacter*, and *Marinobacterium* exhibited significantly higher LDA scores in the UV/PMS–HAA system, indicating enhanced capacities for organic removal and nitrogen assimilation under the combined oxidative and aerobic treatment regime. The Kruskal–Wallis test (Fig. S9) exhibited significant variation among sampling points, with dynamic shifts in *Halomonas*, *Marinobacter*, *Soehngenia*, and *Corynebacterium*. UV/PMS pre-oxidation reshaped microbial structure, promoting oxidative stress–adapted taxa better suited for high-salinity leachate treatment via heterotrophic ammonia assimilation.

### 3.6. Correlation analysis of microbial communities and environmental factors

The connections in Fig. 4A illustrate the significant associations between dominant microbial genera and key environmental and functional parameters. Several key genera—including *Halomonas*, *Marinobacter*, and *Marinobacterium*—exhibited strong positive correlations ($P < 0.01$) with both COD removal and N removal, highlighting their pivotal roles in organic degradation and nitrogen assimilation under UV/PMS–HAA conditions. These genera were known for their redox adaptability and versatile metabolism, which aligned with their enrichment during advanced oxidation processes and their association with ammonium assimilation enzymes such as GS and GDH. *Halomonas* was significantly correlated with TAA and GS activity ($P < 0.001$), supporting its function in transaminase-driven ammonium assimilation, reflected the metabolic integration of carbon and nitrogen pathways, facilitated by oxidative stress–resilient taxa. *Marinobacter* also showed associations with Component 4 (humic-like substances) and GOGAT, implying a role in the oxidative breakdown of recalcitrant DOM and subsequent nitrogen uptake. Notably, the correlations between microbial genera and *Glu/Gln*-related enzymes (*GS*, *GDH*, and *GOGAT*) were robust and statistically significant ($P < 0.01$), underscoring the central role of the *Glu/Gln* cycle in ammonium assimilation.

Mantel test (Fig. 4A) indicated significant correlations among key environmental/biochemical indicators (Han et al., 2023). Moderate correlations were also observed with Component 3 and PN, highlighting the indirect influence of gene expression on carbon–nitrogen coupling. Significant associations were found with $NH_4^+$–N removal, Component 3, Component 4, PN, GDH, GS, Glu, and especially TAA ($P < 0.05$), suggesting that enzymatic activity directly mediates the conversion of DOM into bioavailable nitrogen forms. Procrustes analysis (Fig. 4B) showed strong correlations between microbial communities and nitrogen ($M^2 = 0.6297$, $P = 0.001$) and carbon metabolism genes ($M^2 = 0.6735$, $P = 0.001$) in the UV/PMS-HAA (Zhao et al., 2024b)., indicating that UV/PMS pretreatment enhanced substrate availability, promoted ammonium-assimilating taxa, and fostered a more functionally integrated microbial community for efficient C-N coupling.

### 3.7. In–depth analysis of microbial communities

The microbial co–occurrence network analysis provided deeper insights into the interactive ecological structures underlying the UV/PMS–HAA and Only HAA (Fig. S10). The UV/PMS–HAA network was characterized by a slightly reduced number of nodes (204 vs. 212) and edges (1304 vs. 1335) compared to the Only HAA, and exhibited a markedly higher proportion of positive correlations (71.91 %), suggesting that oxidative pretreatment promoted cooperative and potentially syntrophic interactions among microbial genera. In the UV/PMS–HAA network, Module 1 accounted for 15.69 % of the community and included hub genera such as *RBG–16–49–21*, *Corynebacterium*, and *Proteiniclasticum*. *Corynebacterium* was known for its robust ammonium assimilation capacity and resilience under oxidative stress, which

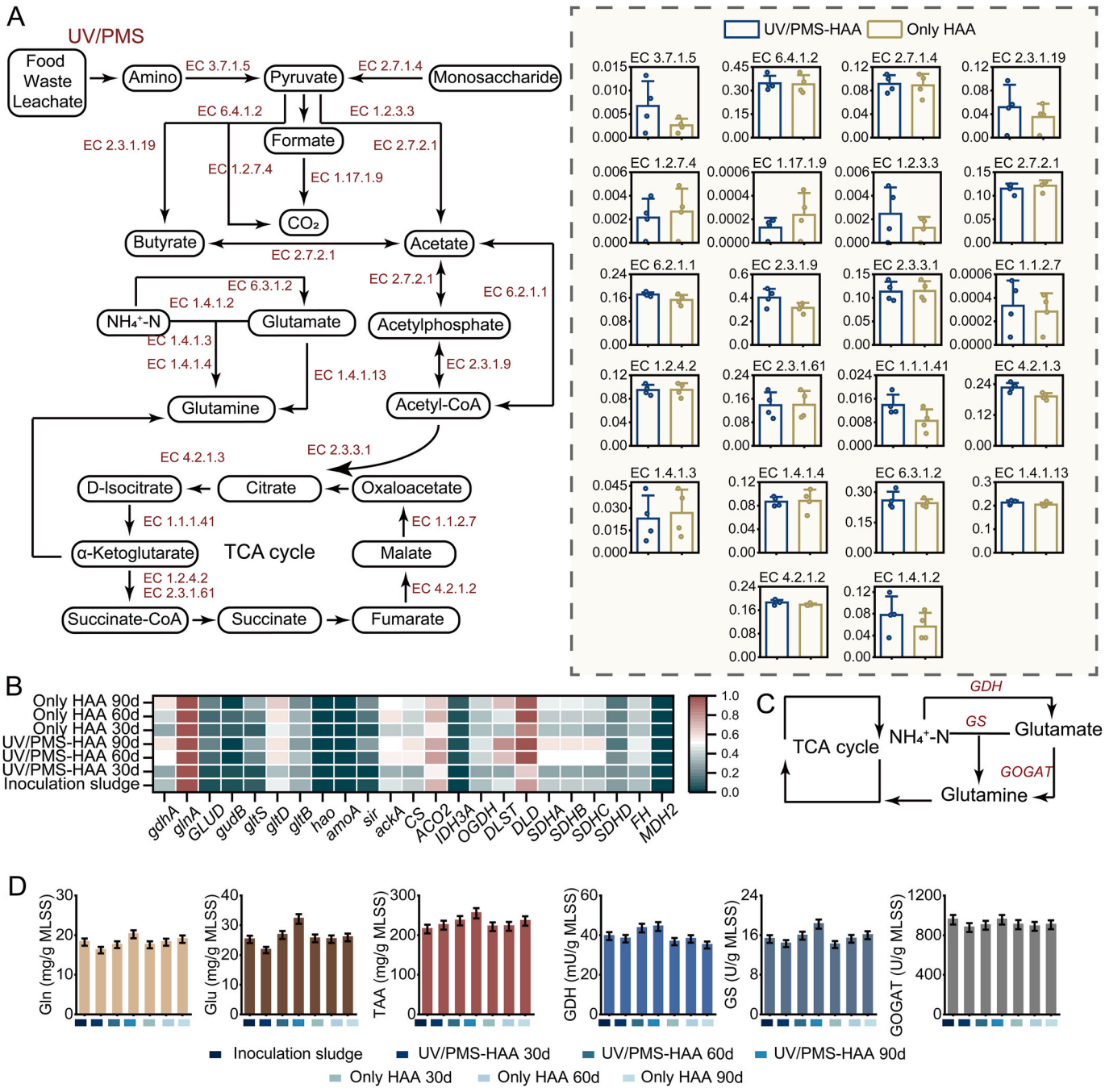


**Fig. 5.** Mechanism analysis: (A) Metabolic pathway and enzyme activity predicted by PICRUSt. (B) The relative abundances of the nitrogen and carbon genes predicted by PICRUSt. The enzyme activity and amino acids of assimilation pathways: (C) mechanism diagram and (D) content.

aligned with its central role in the UV/PMS–HAA network. *Proteiniclasticum* may contribute to the breakdown of peptides and proteins into assimilable nitrogen sources, thereby facilitating the HAA pathway (Wang et al., 2025a). *RBG–16–49–21* had been associated with hydrocarbon degradation and appeared to form tight cooperative linkages within the network. The presence of *Stappia* and *A4b* in distinct modules further illustrated functional partitioning; *Stappia* was the ability to remove refractory organic substances (Han et al., 2022), while *A4b* may be involved in the degradation of recalcitrant DOM components (Li et al., 2025). The Only HAA network demonstrated a higher proportion of negative correlations (36.43 %), implying a more competitive microbial environment. Genera such as *Marinobacter*, *Pseudomonas*, and *Marinicella* were identified as central taxa in this system, particularly in Module 1 and Module 2. *Pseudomonas* was a well–known versatile genus with broad metabolic capabilities, including nitrate reduction and hydrocarbon degradation (Wu et al., 2025). *Marinicella* and *Proteiniclasticum* also played prominent roles in Only HAA but engaged in a greater number of antagonistic interactions.

Robustness analysis (Fig. S11) revealed that the UV/PMS–HAA microbial network exhibited higher natural connectivity and average degree than the Only HAA. Oxidative pretreatment promoted more redundant and resilient microbial interactions, likely driven by increased cooperative associations among genera involved in organic nitrogen transformation, thereby supporting sustained functional performance under environmental disturbances. The neutral community model (Fig. S12) indicated a limited fit for both UV/PMS–HAA and Only HAAs ($R^2$ = 0.035 and 0.042, respectively), suggesting that deterministic processes predominantly governed microbial assembly. The

selective pressure imposed by UV/PMS pretreatment and subsequent HAA conditions shaped specific microbial interactions, favoring the enrichment of functionally synergistic genera involved in nitrogen assimilation and organic matter degradation. The triangular plot (Fig. S13) revealed that species replacement (Rep) was the dominant process in the UV/PMS-HAA, suggesting strong deterministic selection by oxidative stress and substrate shifts, promoted the enrichment of nitrogen-assimilating taxa, enhancing microbial stability and functional resilience. Fig. S14 shows that microbial communities in the UV/PMS-HAA had significantly narrower niche breadths, indicating a dominance of metabolic specialists. In contrast, the Only HAA supported broader niches and more generalists. UV/PMS pretreatment created a selective environment, enriching specialized taxa and enhancing functional stability and resilience. SIMPER analysis (Fig. S15) revealed a 59.2 % OTU difference between the two systems, indicating that advanced oxidation reshaped microbial assembly by selecting metabolically specialized taxa, thereby enhancing functional divergence, synergistic interactions, and system specialization.

### 3.8. Metabolic mechanism analysis

#### 3.8.1. Metabolic pathway and enzyme activity

The enzyme activity (Fig. 5A) demonstrated that coupling UV/PMS advanced oxidation with aerobic heterotrophic ammonium assimilation significantly influenced the microbial metabolic landscape, especially regarding substrate utilization and nitrogen metabolism pathways. Notably, the activity of EC 3.7.1.5—an enzyme linked to the hydrolytic cleavage of amino acids (Guo et al., 2023) —was markedly higher in the UV/PMS–HAA system (0.00674 ± 0.00525 %) compared to the Only HAA (0.00259 ± 0.00144 %). The oxidative pretreatment generated a greater abundance of low–molecular–weight aromatic intermediates, thereby selecting for microorganism possessing the enzymatic machinery to degrade such compounds. Further, EC 2.3.1.9 (acetyl–CoA C–acetyltransferase) and EC 6.2.1.1 (long–chain–fatty–acid—CoA ligase), both essential for lipid and fatty acid metabolism, were significantly upregulated in the UV/PMS–HAA. These enzymes were critical in β–oxidation and acetyl–CoA production, which fuel energy metabolism and biosynthesis under carbon–limited or stress–induced conditions (Usman et al., 2022). The functional enrichment of microbial groups capable of exploiting fatty acid intermediates was released through PMS–induced oxidation.

The key enzymes in central nitrogen metabolism—such as EC 1.4.1.2 (glutamate dehydrogenase), EC 1.4.1.13 (glutamate synthase), and EC 6.3.1.2 (glutamine synthetase)—exhibited only modest differences between the two systems, albeit with slightly higher activity in the UV/PMS–HAA. While the oxidative pretreatment had a profound effect on carbon substrate availability and related enzymatic responses, it subtly enhanced nitrogen assimilation pathways (Zhao et al., 2025b). Importantly, this functional stability in nitrogen–transforming enzymes may contribute to the robustness of ammonium assimilation despite chemical pre–oxidation, indicating resilience in microbial nitrogen utilization capacity (Zhao et al., 2023a). Moreover, EC 2.3.1.19 (malonyl–CoA:ACP transacylase) and EC 4.2.1.3 (aconitate hydratase), central to the TCA cycle, also showed elevated activities in the UV/PMS–HAA (Wang et al., 2025b). The increased metabolic flux through central carbon metabolism, likely to support both detoxification of oxidation byproducts and biomass regeneration. In the UV/PMS–HAA system, enhanced activities of key enzymes involved in the tricarboxylic acid (TCA) cycle, such as EC 1.2.4.2 (pyruvate dehydrogenase) and EC 1.1.1.41 (isocitrate dehydrogenase), were observed, indicating an intensified central carbon metabolism (Liang et al., 2025). These enzymes were essential for converting pyruvate into acetyl–CoA and further catalyzing the oxidative decarboxylation of isocitrate, respectively, thereby facilitating efficient energy production and carbon flow.

#### 3.8.2. Functional genes related to carbon and nitrogen

The functional gene abundance (Fig. 5B) revealed a distinct enhancement of nitrogen assimilation and TCA cycle activity in the UV/PMS–HAA system. In nitrogen assimilation, *glnA* (glutamine synthetase) showed a marked increase from 0.0163 % in the Only HAA to 0.1350 % in the UV/PMS–HAA system, while *gdhA* (glutamate dehydrogenase) similarly was increased from 0.0078 % to 0.0576 %. Furthermore, *gltD* and *gltB*, encoding subunits of glutamate synthase (Zhao et al., 2023c), were elevated to 0.0666 % and 0.0393 % in the UV/PMS–HAA system, compared to 0.0042 % and 0.0086 %, respectively, in the Only HAA. These genes coordinated the glutamine–glutamate loop, a central pathway for incorporating ammonium into organic nitrogen compounds under aerobic heterotrophic conditions (Zhao et al., 2024b). Additionally, *GLUD* and *gltS* was increased by 2.94– and 1.98–fold, respectively, further emphasizing the enhanced nitrogen assimilation capacity induced by UV/PMS pretreatment. The *amoA* gene, responsible for ammonia oxidation, was undetectable in both systems, and *hao* abundance remained negligible ($1.74 \times 10^{-5}$ in UV/PMS–HAA; $5.57 \times 10^{-7}$ in Only HAA).

Genes involved in carbon metabolism, particularly the TCA cycle, also displayed significantly higher abundance in the UV/PMS–HAA system. *ACO2* (aconitase) increased from 0.0118 % in Only HAA to 0.0922 % in UV/PMS–HAA; *OGDH* (oxoglutarate dehydrogenase) rose from 0.0026 % to 0.0496 %; and *DLST* and *DLD*, encoding subsequent TCA cycle enzymes, were elevated to 0.0725 % and 0.1137 %, respectively—representing 8.96– and 9.8–fold increases compared to Only HAA. Notably, all four subunits of succinate dehydrogenase (*SDHA–D*) exhibited higher expression in the UV/PMS–HAA, particularly *SDHA* (0.0575 % vs. 0.0019 %) and *SDHB* (0.0573 % vs. 0.0020 %).

#### 3.8.3. Assimilative key substances

Three enzymes central to the assimilation process—*GDH*, *GOGAT*, and *GS*—exhibited differential activities over time, correlating with variations in their respective metabolic products, including Glu, Gln, and TAA (Fig. 5C). In the UV/PMS–HAA system, *GDH* activity increased progressively from 38.21 ± 1.91 mU/g MLSS at 30 days to 44.32 ± 2.22 mU/g MLSS at 90 days. Enhanced direct assimilation of $NH_4^+$–N into Glu via the *GDH* pathway under oxidative preconditioning. Meanwhile, *GOGAT* activity in UV/PMS–HAA maintained high stability, peaking at 956.21 ± 47.81 U/g MLSS at day 90, matching the initial inoculation sludge level, indicated a sustained flux through the *GS–GOGAT* cycle. *GS* activity also rose markedly, reaching 18.21 ± 0.91 U/g MLSS at day 90, suggesting enhanced ATP–dependent conversion of $NH_4^+$–N into Gln. Correspondingly, metabolic products in UV/PMS–HAA showed increasing accumulation. Glu concentration increased from 21.66 ± 1.08 mg/g MLSS at day 30–32.12 ± 1.61 mg/g MLSS at day 90, while Gln reached 20.21 ± 1.01 mg/g MLSS. The TAA content peaked at 255.21 ± 12.76 mg/g MLSS, representing the highest level among all time points and systems. In contrast, the Only HAA showed more limited enhancement. *GDH* activity declined slightly at day 90 (35.04 ± 1.75 mU/g MLSS), suggesting a weaker HAA pathway. Although *GOGAT* activity remained relatively high (905.33 ± 45.27 U/g MLSS), *GS* activity did not exhibit significant upregulation, remaining at 15.99 ± 0.80 U/g MLSS. Metabolite levels such as Glu (25.92 ± 1.30 mg/g MLSS) and Gln (18.99 ± 0.95 mg/g MLSS) remained lower than in the UV/PMS–HAA system. Notably, TAA content at day 90 (235.69 ± 11.78 mg/g MLSS) was significantly lower than that of the UV/PMS–HAA system. Pre-oxidative modification of the wastewater matrix likely enhanced nitrogen bioavailability and redox balance, promoting coordinated GDH and GS-GOGAT pathway activity and amino acid biosynthesis in the UV/PMS-HAA system.

### 3.9. Heterotrophic ammonia assimilation contribution calculation

Fig. S16 shows the PLS–PM analysis of key interactions in the UV/PMS–HAA and Only HAAs. In the UV/PMS–HAA system, functional

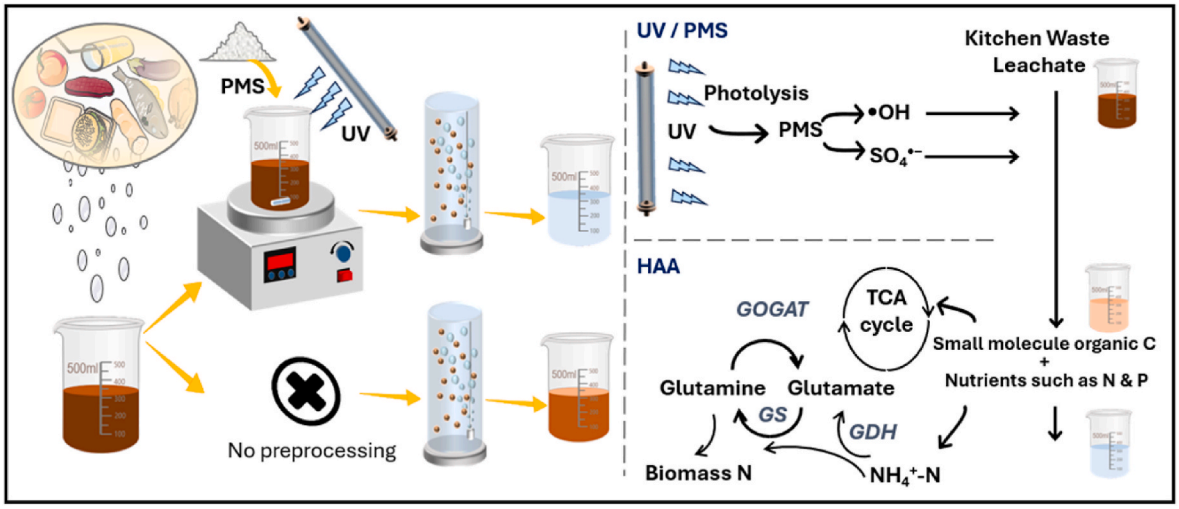


**Fig. 6.** Schematic diagram of degradation mechanism.

microorganisms strongly promoted product formation (0.697) and indirectly enhanced COD (0.412), $NH_4^+$–N (0.319), and EPS removal via metabolites. Biomass-derived products played a central role in linking microbial activity to pollutant degradation. The COD → $NH_4^+$–N → EPS cascade (1.038, 0.675) highlights strengthened carbon–nitrogen coupling under oxidative pretreatment. In contrast, the Only HAA showed weaker, inconsistent relationships. UV/PMS integration thus enhanced removal efficiency by fostering synergistic microbe–enzyme–metabolite interactions.

### 3.10. Degradation mechanism analysis

Fig. 6 revealed the reaction mechanism and pollutant degradation mechanism of UV/PMS–HAA system. UV/PMS generated sulfate ($SO_4^{\bullet-}$) and hydroxyl radicals (•OH), both of which were highly reactive and capable of breaking down complex macromolecular organics into smaller, more biodegradable compounds. These oxidation reactions resulted in the formation of carboxylic acids, alcohols, and other small organic molecules, which served as readily available carbon sources for microbial metabolism (Yin and Wang, 2022). The enhanced ammonia removal observed in the UV/PMS–HAA system can be attributed to the improved availability of organic carbon substrates for microbial uptake. The heterotrophic ammonia assimilation pathway incorporated ammonia into biomass through the glutamine synthetase and glutamate dehydrogenase pathways. In this process, ammonia was directly assimilated into microbial biomass rather than being oxidized to nitrate, which minimized nitrogen losses and enhances nitrogen recycling within the system (Zhao et al., 2024a). The increased availability of biodegradable carbon sources from UV/PMS oxidation further promotes microbial growth and nitrogen uptake efficiency.

However, the high concentrations of organic carbon and nitrogen in leachate may lead to the formation of carbonaceous and nitrogenous disinfection by-products (DBPs) during the advanced oxidation process involving UV-activated PMS. Although trace levels of DBPs (typically in the ng/L range) may be generated during UV/PMS treatment, the impact of DBPs was no significant impact on the treatment efficiency of major pollutants and no significant inhibitory effect on microbial activity. Based on the principle of minimizing environmental impact, it is necessary to use activated carbon or membrane separation technology in series after this research process to deeply degrade and remove DBP in practical applications.

## 4. Conclusions

In this study, the UV/PMS pre–oxidation step played a pivotal role in rebuilding microbial assembly and metabolic pathways during food waste leachate treatment, achieving 35.6 % higher $NH_4^+$–N removal than the control. Tighter EPS structure and improved sludge morphology facilitated microbial retention and process stability. Microbial diversity was enriched, with UV/PMS–HAA promoting deterministic assembly and strong positive interactions among key genera. By selectively enriching functional taxa with narrow niches and strong assimilation potential, it promoted deterministic community succession and elevated expression of key heterotrophic ammonium assimilation genes (*glnA*, *gdhA*). This study highlights the critical value of advanced oxidation in steering nitrogen metabolism and optimizing biological treatment for high–strength organic wastewater.

## CRediT authorship contribution statement

**Chuanfu Zhao:** Writing – original draft, Data curation. **Wenhao Zhang:** Data curation. **Jianhua Lei:** Data curation. **Fei Han:** Data curation. **Mengru Zhang:** Data curation. **Yiting Guo:** Data curation. **Yuke Li:** Writing – review & editing. **Weizhi Zhou:** Writing – review & editing, Supervision, Funding acquisition.

## Declaration of competing interest

The authors declare that they have no known competing financial interests or personal relationships that could have appeared to influence the work reported in this paper.

## Acknowledgments

This work was supported by National Key R&D Program of China (2022YFC2807503); National Natural Science Foundation of China (U1906221).

## Appendix A. Supplementary data

Supplementary data to this article can be found online at https://doi.org/10.1016/j.envres.2025.122481.

## Data availability

Data will be made available on request.

## References


Babu Ponnusami, A., et al., 2023. Advanced oxidation process (AOP) combined biological process for wastewater treatment: a review on advancements, feasibility and practicability of combined techniques. Environ. Res. 237, 116944.

Cai, G., et al., 2022. Control for chlorine resistant spore forming bacteria by the coupling of pre-oxidation and coagulation sedimentation, and UV-AOPs enhanced inactivation in drinking water treatment. Water Res. 219, 118540.

Gao, L., et al., 2023. Combination of partial nitrification and microbial fuel cell for simultaneous ammonia reduction, organic removal, and energy recovery. Bioresour. Technol. 386.

Gao, R., et al., 2025. Removal of disinfection residual bacteria in UV(222), UV(222)/H(2)O(2) and UV(222)/peroxymonosulfate systems: what is the safe usage for wastewater reclamation. Water Res. 282, 123602.

Garnier, C., et al., 2023. Water reuse in the food processing industries: a review on pressure-driven membrane processes as reconditioning treatments. J. Food Eng. 344.

Gunde-Cimerman, N., et al., 2018. Strategies of adaptation of microorganisms of the three domains of life to high salt concentrations. FEMS Microbiol. Rev. 42, 353–375.

Guo, H., et al., 2023. Reduced sulfide and methane in rising main sewer via calcium peroxide dosing: insights from microbial physiological characteristics, metabolisms and community traits. J. Hazard Mater. 451, 131138.

Han, F., et al., 2022. Cooperation of heterotrophic bacteria enables stronger resilience of halophilic assimilation biosystem than nitrification system under long-term stagnation. Sci. Total Environ. 848, 157806.

Han, F., et al., 2023. Responses of halophilic microbial communities to changes in salt composition: Comparison between autotrophic nitrification and heterotrophic ammonia assimilation biosystems. Bioresour. Technol. 386, 129500.

Igwegbe, C.A., et al., 2024. Sustainable municipal landfill leachate management: current practices, challenges, and future directions. Desalination Water Treat. 320.

Jiao, T., et al., 2024. Recovery of ammonia assimilating microbiome after Cr (VI) shock by bio-accelerators. J. Environ. Manag. 370, 123020.

Khanthong, K., et al., 2021. Microbial diversity of marine shrimp pond sediment and its variability due to the effect of immobilized media in biohydrogen and biohythane production. J. Environ. Chem. Eng. 9.

Lang, L., et al., 2020. Awareness of food waste recycling in restaurants: evidence from China. Resour. Conserv. Recycl. 161.

Lei, J., et al., 2024. New insight in the biotreatment of produced water: Pre-oxidation paves a rapid pathway for substrate selection in microbial community. J. Hazard. Mater. 480, 136483.

Li, J., et al., 2018. System performance and microbial community succession in a partial nitrification biofilm reactor in response to salinity stress. Bioresour. Technol. 270, 512–518.

Li, J., et al., 2025. Anammox-induced magnesium phosphate mineralization for digestate treatment: organic matter intervention and elemental flow. Chem. Eng. J. 504.

Liang, X., et al., 2025. Using excitation-emission matrix-parallel factor analysis to access the effect of temperature parameters on the humification of community kitchen waste compost. Biomass Bioenergy 197.

Lin, X., et al., 2024. Mechanistic insight into assimilation capture: implication for high-efficiency nitrogen removal from mature landfill leachate. Chem. Eng. J. 498.

Masouleh, S.Y., et al., 2024. Landfill leachate treatment using sequential natural zeolite adsorption and peroxymonosulfate activated by UV/Fe2+ system: effects of main operating parameters and application of fluorescence EEM to monitor organic matters' transformation. J. Environ. Chem. Eng. 12.

Qin, S., et al., 2025. Comparison of the start-up of rotating biofilm contactor reactor with HN-AD bacteria inoculation under high and low influent ammonia conditions. J. Environ. Manag. 381, 125206.

Srivastava, A., et al., 2021. Treatment of saline wastewater using physicochemical, biological, and hybrid processes: insights into inhibition mechanisms, treatment efficiencies and performance enhancement. J. Environ. Chem. Eng. 9, 105775.

Sun, Y., et al., 2024. Impacts of electric field coupled membrane bioreactor on phenol wastewater with high salinity: performance, membrane fouling and eco-friendly strategy. J. Water Proc. Eng. 60.

Usman, M., et al., 2022. Microbial beta-oxidation of synthetic long-chain fatty acids to improve lipid biomethanation. Water Res. 213, 118164.

Wang, J., Wang, S., 2018. Activation of persulfate (PS) and peroxymonosulfate (PMS) and application for the degradation of emerging contaminants. Chem. Eng. J. 334, 1502–1517.

Wang, Q., et al., 2025a. Study on short-chain fatty acids production from anaerobic fermentation of waste activated sludge pretreated by alkali-activated ammonium persulfate. Bioresour. Technol. 428, 132461.

Wang, Z., et al., 2025b. Effects of Fe3O4 on production of even-carbon volatile fatty acids by anaerobic fermentation of kitchen waste under ultrasonic-alkali pretreatment: performance, metabolic functions, and metabolic pathways. J. Environ. Chem. Eng. 13.

Wu, J., et al., 2025. Recruiting high-efficiency denitrifying consortia using Pseudomonas aeruginosa. Water Res. 277, 123303.

Yang, Y., et al., 2025. Unleashing the potential of biomass-doped sludge biochar: promotion of persulfate activation by biochar-derived dissolved organic matter. Separ. Purif. Technol. 361.

Yin, Q., et al., 2024. Highly efficient removal of contaminant from typical dye wastewater by using individual AOPs-A/O processes: design, performance, and mechanism. J. Environ. Chem. Eng. 12.

Yin, Y., Wang, J., 2022. Production of medium-chain carboxylic acids using sewage sludge pretreated by combined Fenton and persulfate oxidation. J. Clean. Prod. 369.

Zhang, B., et al., 2025a. Impaired denitrification of aerobic granules in response to micro/nanoplastic stress: insights from interspecies interactions and electron transfer processes. Water Res. 279, 123472.

Zhang, M., et al., 2022. The effect of salinity on ammonium-assimilating biosystems in hypersaline wastewater treatment. Sci. Total Environ. 829.

Zhang, M., et al., 2021a. Nitrogen recovery by a halophilic ammonium-assimilating microbiome: a new strategy for saline wastewater treatment. Water Res. 207, 117832.

Zhang, Q., et al., 2025b. Analysis strategy of contamination source using chemical fingerprint information based on GC-HRMS: a case study of landfill leachate. Water Res. 273, 123067.

Zhang, X., et al., 2021b. A nitrogen supplement to regulate the degradation of petroleum hydrocarbons in soil microbial electrochemical remediation. Chem. Eng. J. 426.

Zhao, C., et al., 2024a. Carbon sources influence on heterotrophic ammonia assimilation: performance and mechanism. Chem. Eng. J. 497.

Zhao, C., et al., 2024b. Nutrients recovery by coupled bioreactor of heterotrophic ammonia assimilation and microbial fuel cell in saline wastewater. Sci. Total Environ. 918, 170697.

Zhao, C., et al., 2023a. Novel strategy for treating high salinity oilfield produced water: Pyrite-activated peroxymonosulfate coupled with heterotrophic ammonia assimilation. Water Res. 247, 120772.

Zhao, C., et al., 2022. Coupling of submersible microbial fuel cell into aerobic granular sludge bioreactor for ciprofloxacin stress alleviation: performance and mechanism. J. Clean. Prod. 373.

Zhao, C., et al., 2023b. Solid slow-release carbon source assembled microbial fuel cell for promoting superior nitrogen removal in an aerobic granular sludge bioreactor. J. Environ. Manag. 325, 116430.

Zhao, C., et al., 2021. Coupling of nitrifying granular sludge into microbial fuel cell system for wastewater treatment: system performance, electricity production and microbial community shift. Bioresour. Technol. 326, 124741.

Zhao, C., et al., 2025a. Aeration-driven regulation of heterotrophic ammonia assimilation under high salinity: Carbon-Nitrogen conversion and microbial community. J. Environ. Chem. Eng., 117911

Zhao, C., et al., 2025b. Flocculent sludge outperforms filler biofilm for high salinity oilfield produced water treatment: performance, metabolic pathways, and microbial communities. J. Hazard Mater. 492, 138217.

Zhao, F., et al., 2023c. Molecular level insight of thiocyanate degradation by Pseudomonas putida TDB-1 under a high arsenic and alkaline condition. Sci. Total Environ. 874, 162578.

Zheng, X., et al., 2025. Halomonas fermentation promoted the biotransformation of active substances from Dictyophora indusiata pileus and the enhancement of antioxidant capacity. Food Biosci. 68.